Journal of Applied Mechanics and Technical Physics, Vol. 36, No. 2, 1995

EVOLUTION OF INTERNAL STRUCTURE OF A LIQUID DESTRUCTION ZONE UNDER IMPULSIVE LOADING

A. R. Berngardt, V. K. Kedrinskii, and E. I. Pal'chikov

UDC 532.538

The dynamic destruction of liquids manifests a number of unique features in contrast to analogous processes in solids. Among these are: 1) rise and development near the free surface of a large cavitation zone [1, 2] for impulsive loading by a shock wave; 2) formation of split foam structure layers [1]; 3) excess by orders of magnitude of the characteristic times of process development as compared to the duration of the loading wave [3, 4]; 4) uncertainty in location of the breakoff point and impossibility of fixing the final state of the specimen.

The process of cavitation failure as a whole can be divided into the following stages [5]: growth of microbubbles, leading to formation of a cavitation zone; zone development up to formation of a foam type structure [3]; destruction of the foam due to dispersion. The cavitation zone is optically opaque for the major portion of its existence. The formation of large scale discontinuities in the liquid due to bubbles merging is an important part of the failure process, which, because of mathematical difficulties, has yet to be studied. Use of pulsed x-ray photography for study of optically opaque cavitation zones was proposed in [3]. The series of x-ray exposures of the cavitation process development allowed tracking the dynamics of the external state of the liquid specimen and study of the character of the process's dependence on loading parameters [6]. When used with special markers, this same method allows tracking the dynamics of mass velocities in the cavitation zone.

The present study will describe methods for, and present results from, computer processing of x-ray exposures obtained in experiments on shock wave loading of a water specimen. The x-ray processing method involves transformation of the images into digital form, input of that data into a computer, and subsequent processing with a specially designed program, with the final goal of extracting quantitative information on the internal structure and dynamics of cavitation zone density in this stage of macrocavity formation. The results of processing a series of x-rays will be presented in the form of density fields in gray-scale representation.

Note that according to [6, 7], two possible cavitation development regimes exist. The process may be reversible, with the cavitation bubbles formed finally collapsing and the specimen becoming transparent again. When critical values of shock wave intensity are exceeded, the bubble growth process becomes irreversible, which leads to formation of a foam structure. The experimental results presented below on cavitation failure of a water specimen were obtained at loading parameter values close to critical.

The essence of the method is division of the object into a finite number of elementary volumes, the density in which is calculated from the digitized x-ray data on the basis of absorption laws and photometric relationships. The process as a whole is symmetric relative to the shock tube axis, so we may limit ourselves to a mean density $\bar{\rho}(z, r)$. In the processing it is assumed that:

1) X-ray beam divergence and change in spectrum can be neglected within the limits of the specimen, and a linear absorption law applies:

$$dI = -I\mu\rho\, dx, \quad I = I_0 \exp(-\mu\rho x); \tag{1}$$

*This study was performed with financial support from the Russian Fund for Fundamental Studies (Project Code 93-013-16383).

M. A. Lavrent'ev Institute of Hydrodynamics, Siberian Division of the Russian Academy of Sciences, Novosibirsk.
Translated from Prikladnaya Mekhanika i Tekhnicheskaya Fizika, No. 2, pp. 99-105, March-April, 1995. Original article submitted December 21, 1993; revision submitted April 14, 1994.

0021-8944/95/3602-0234$12.50

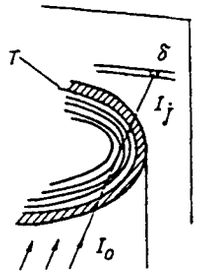

Fig. 1

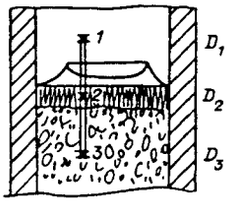

Fig. 2

2) the photometric density of the x-ray lies within the linear portion of the material's sensitometry curve, i.e., the law

$$D_1 - D_2 = \gamma \lg(E_1/E_2) \tag{2}$$

is valid for any two points of the image field. Here γ = const is the contrast coefficient; E_k, D_k are the exposure and photometric density at the point k. The path of an elementary beam of intensity I_0 (Fig. 1) through the cylindrical specimen contained in the shock tube T consists of elementary segments which are the intersection of the ray line of the concentric rings composing the specimen cross section. The radiation passing through the specimen and falling upon the film creates an image composed of corresponding pixel elements of a size equal to the cross section of the elementary beam. We will denote the value of the mean medium density in ring i by $\bar{\rho}_i$, so that for ray j the beam intensity upon exit from the tube will have the form

$$I_j = I_0 \exp(-2\rho\mu_t x_{tj} - 2\sum \bar{\rho}_{ij}\mu_{ij}x_{ij}), \tag{3}$$

where μ is the effective mass radiation absorption coefficient, dependent on the effective radiation energy and varying for elementary rays which have traversed the filter (shock tube wall) and cavitating specimen (in view of its insignificance, we neglect absorption in air); x_{ij} is the path of ray j in ring i of the liquid specimen; x_{tj} its path in the shock tube wall; ρ, $\bar{\rho}_{ij}$ are the density of the wall material and the medium in ring i of ray j respectively. It is considered here that each ring (except the outermost) is cut by the ray twice. The summation in Eq. (3) is performed over the number or rings i, which is dependent on the position of the intersecting ray j.

We will consider three elements of a projection located on a single straight line parallel to the object's axis of symmetry (Fig. 2). Using Eqs. (1) and (2) with consideration of Eq. (3), we obtain for these three points the following relationship for the photographic densities D_k(k = 1, 2, 3):

$$\frac{D_3 - D_1}{D_2 - D_1} = \frac{(\mu\sum\bar{\rho}_{ij}x_{ij})_3 - (\mu\sum\bar{\rho}_{ij}x_{ij})_1}{(\mu\sum\bar{\rho}_{ij}x_{ij})_2 - (\mu\sum\bar{\rho}_{ij}x_{ij})_1}. \tag{4}$$

Writing N relationships of the form of Eq. (4) for N elements of the section projection, we have a system of equations for $\bar{\rho}$, and if δ is the number of pixels and R is the external tube radius, then $N\delta$ = R. If the density and configuration are known for the object points, the projections of which lie at points 1 and 2, then the quantities $(\bar{\rho}_{ij})_{1,2}$ are known, and $(x_{ij})_k$ can be

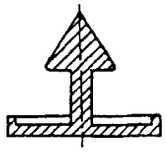

Fig. 3

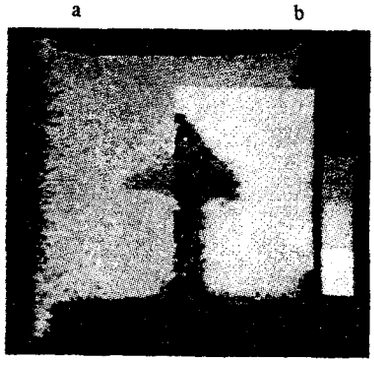

Fig. 4

found geometrically. In the given case the region denoted by the index 1 corresponds to air layers, so that terms with this index may be neglected in Eq. (4). There remain N unknowns $(\bar{\rho}_{ij})_3$, for which we solve system (4). Such operations are carried out in each section of the entire volume. Note that the physical constants γ and μ are abbreviated in the final expressions and only the experimental values of D_k are used for the calculations.

To verify the validity of the calculations, estimate the resolving power of the method, and determine correspondence of the results to reality, a calculation of the density of a test object was carried out. This object was a figure of rotation 30 mm in diameter and 32 mm high, made of foamed plastic with a density $<<$ 1 g/cm^3 (Fig. 3). X-ray films of the object in a water-filled shock tube (outer diameter 30 mm, wall thickness 5 mm) were digitized using the FEAG digitizer of the computation center of the Siberian Branch of the Russian Academy of Sciences. The digitizer scans the film with an 80 μ diameter laser beam. The digitized data were recorded on magnetic tape and used for processing by the method described above. The density field was displayed graphically on a raster display screen in gray scale. A photograph of the display screen is shown in Fig. 4, where together with the digitized image (a) the corresponding symmetrical portion of the density distribution is shown (b). It is evident that in the portions of the original photograph near the tube walls the shape of the specimen was not scanned. Calculation of the density field yields a shape (Fig. 4b) which agrees satisfactorily with the original of Fig. 3.

To estimate the accuracy of reproduction of the test image the mean square deviation

$$\sigma = \sqrt{\left[\sum_1^N (f_i - \bar{f}_i)^2\right]/(N-1)}$$

was calculated for points of the test object. For $\bar{f}_i$ the value 0.5 g/cm^3 was used, since the density of the object $\rho_0 \approx 0$ while the density of the medium $\rho_c = 1$ g/cm^3. For the points of the inclined boundary $\sigma \approx 0.1$ g/cm^3, for the points of the object near the shock tube wall $\sigma = 0.135$ g/cm^3. Such a deviation is completely satisfactory for the given case when it is considered that during exposure the object was located in the shock tube, which scatters and absorbs approximately half of the radiant flux. Consequently, objects with dimensions of the order $l_0 \approx 0.1(l_c\rho_c\mu_c)/(\rho_0\mu_0)$, are near the threshold of resolution. Here ρ_i, μ_i, l_i are densities, mass absorption coefficients, and dimensions of the object or medium respectively.

A series of x-rays of sequential development of the cavitation zone (Fig. 5) was obtained in an experiment in which a water specimen was loaded by a shock wave with approximately triangular profile with amplitude of $1.75 \cdot 10^7$ Pa and duration

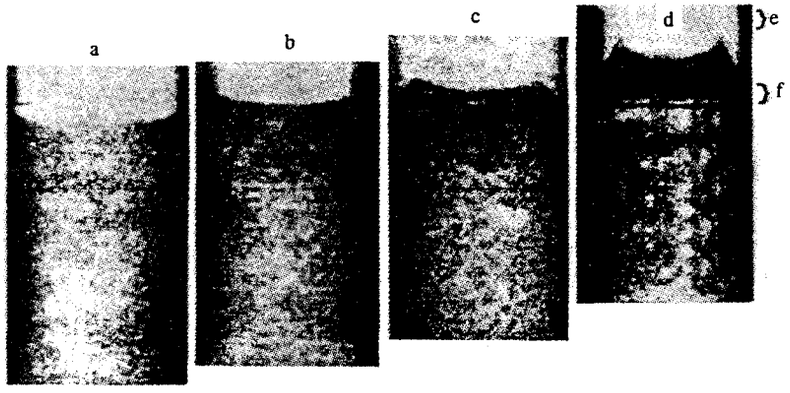

Fig. 5

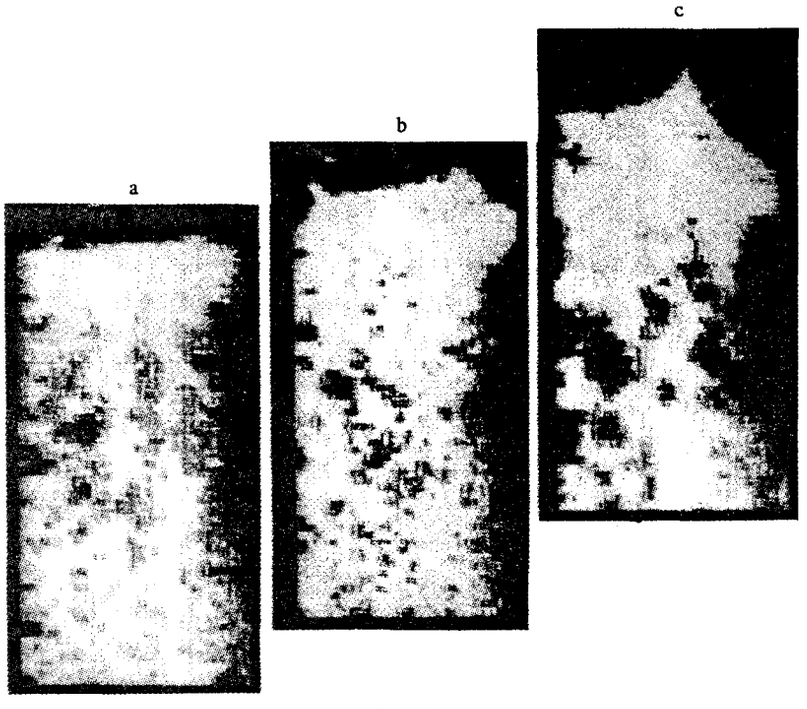

Fig. 6

of 30 μsec. The radiation sources were located along a circle in a plane perpendicular to the shock tube axis at 60° intervals. Figure 5 shows the specimen state before loading (a) and 200, 400, and 800 μsec after exit of the shock wave front to the free surface (b-d).

In calculating the density distribution of the medium a preliminary appodization (averaging) was performed over 3 × 3 matrices of image elements, with local averaging over each 4 × 8 pixel region. This operation allowed reduction in the number of steps and the error introduced into the calculations due to reduction in the grain noise level, with practically no degradation of spatial resolution.

The density distributions obtained were shown on the raster display. Photographs of the density fields are shown in Fig. 6a-c for times of 200, 400, and 800 μsec. A gray-scale interpretation of the density values was used, lighter shades corresponding to higher density areas. The axis of symmetry coincides with the left edge of each image while the right edge is the outer boundary of the specimen. For the calculations segments of the photograph were used depicting portions of the object with known density distributions: a fragment of the tube filled with air, or continuous water (Fig. 5e, f). Photographic density in these segments corresponds to portions of the object with density of either 0 (air) or 1 g/cm^3 (water).

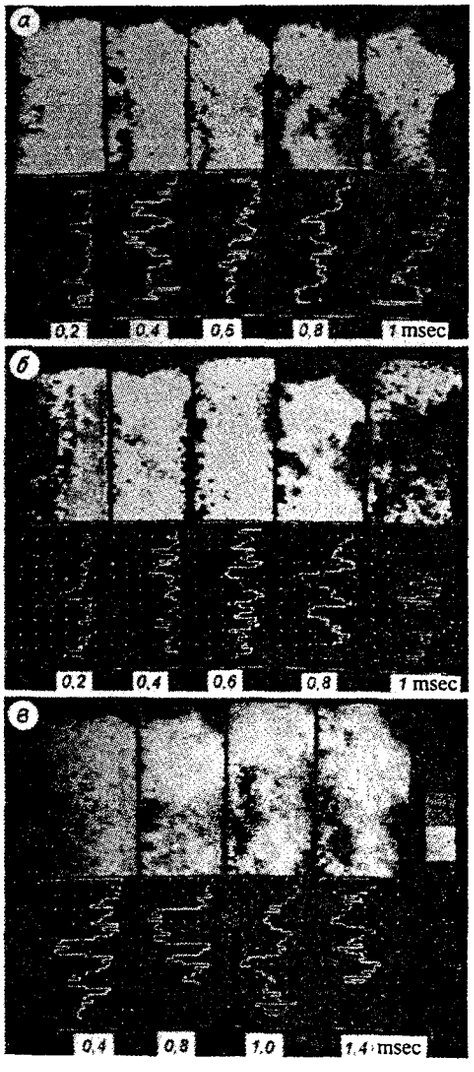

Fig. 7

A series of images was composed from experimental results with identical loading parameters in order to analyze the dynamics of cavitation zone internal structure. Three series of processed images obtained in experiments with most characteristic loading parameters are shown in Fig. 7. Beneath the corresponding density fields graphs are shown with density values along the vertical, taken in a narrow zone 10 elements wide near the axis of symmetry, the left edge of each image, while beneath the graph the time of the exposure is noted, reckoned from the moment of shock wave front exit onto the free surface of the specimen. Each series is composures obtained in two identical experiments.

At the 200 μsec point the specimen state is characterized by the presence of extensive density inhomogeneities (Fig. 7a, b). Figure 7a-c corresponds to experimental results with shock wave duration and amplitude of 50 μsec, $1.5 \cdot 10^7$ Pa, 30 μsec, $1.6 \cdot 10^7$ Pa, and 70 μsec, $1.3 \cdot 10^7$ Pa respectively. At the 400 μsec (Fig. 7a, c) and 600 μsec (Fig. 7b) points macrocavities with densities ≤ 0.1 g/cm^3 are formed. These may be clusters of coarse bubbles or a single macrocavity.

The cavities formed increase in size, and may change in configuration and combine. The combination process can be traced from exposures corresponding to a single experiment, for example those at 400 and 800 μsec (Fig. 7a), 1 and 1.4 msec, 400 and 800 μsec (Fig. 7c), 600 μsec and 1 msec (Fig. 7b). The graphs of vertical density distribution begin at the top; the origin corresponds to the cavitation zone boundary (below zone f of Fig. 5). They have abrupt pulsations, related to the intense inhomogeneity of the zone, and indicate formation of large cavities. The experiments did not establish any regularity in their spatial arrangement.

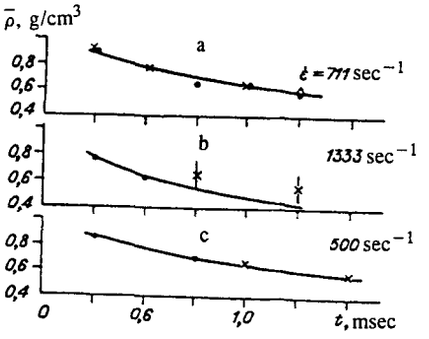

Fig. 8

The time dependences of average density of the medium for the entire zone are monotonic curves for experiments with identical loading parameters. Graphs of this dependence for the experiments of Fig. 7a-c are shown in Fig. 8a-c respectively. The various points refer to different experiments, while the lines denote the dynamics of density as calculated theoretically with the assumption of instantaneous relaxation of tensile stresses behind the rarefaction wave front [8]:

$$\bar{\rho} = \rho_0 \frac{1}{1 + \dot{\varepsilon} t}.$$

It is assumed here that the rate of medium deformation $\dot{\varepsilon}$ is constant and defined by the slope of the pressure decay behind the shock wave front. The graphs show corresponding values from the experimentally recorded pressure profiles.

For loads with parameters $1.6 \cdot 10^7$ Pa, 30 μsec (Fig. 8b) the deviation of the theoretical curve from experimental data can be explained by idealization of the $\bar{\rho}(\dot{\varepsilon}, t)$ relationship.

Experimental confirmation of this dependence makes possible determination of an important parameter of the process — the time required for medium relaxation to the bubble "bulk density" state (volume concentration of the vapor–gas phase in the range 0.5-0.7), which is defined as the transition time in the failure process:

$$t_* \simeq \frac{\rho_0/\bar{\rho} - 1}{\dot{\varepsilon}}.$$

This state of the medium can be defined as lying between a cavitating liquid and a foam structure. It can easily be seen that at $\rho_0/\bar{\rho} = 2$ the relaxation time $t_* \simeq 1/\dot{\varepsilon}$ is determined only by the deformation rate. According to the experimental data, for $\dot{\varepsilon} \simeq 1330$ sec^{-1} the time for relaxation to a foam structure is about 700 μsec, while for $\dot{\varepsilon} \simeq 500$ sec^{-1}, $t_* \approx 2000$ μsec.

The method proposed above for study of two-phase flow structure by processing of x-ray images allows recording of density macroinhomogeneities and the dynamics of macrodiscontinuity formation in an optically opaque cavitating liquid. Density field data provide a unique possibility for analyzing mean values of the local parameters and are an important element in construction of a physical model of the process of liquid failure in intense rarefaction waves.

REFERENCES

1. V. K. Kedrinskii, "Surface effects in underwater explosion (review)," Zh. Prikl. Mekh. Tekh. Fiz., No. 4, 66-87 (1978).
2. V. K. Kedrinskii, "Cavitation zone dynamics in underwater explosion near the free surface," Zh. Prikl. Mekh. Tekh. Fiz., No. 5, 68-78 (1975).
3. I. R. Baikov, A. R. Berngardt, V. K. Kedrinskii, and E. I. Pal'chikov, "Experimental methods for cavitation cluster study," Zh. Prikl. Mekh. Tekh. Fiz., No. 5, 30-34 (1984).
4. N. N. Chernobaev, "Fundamentals of impulsive destruction of liquids with various physical properties," in: Dynamics of Continuous Media, Collected Studies [in Russian], Sib. Otdel. Akad. Nauk SSSR, No. 84 (1988), pp. 135-143.
5. V. K. Kedrinskii, "Nonlinear problems of cavitational liquid destruction under explosive loading (review)," Zh. Prikl. Mekh. Tekh. Fiz., No. 3, 74-90 (1993).

6. A. R. Berngardt, "Dynamics of the cavitation zone in impulsive destruction of water," in: Dynamics of Continuous Media, Collected Studies [in Russian], Sib. Otdel. Akad. Nauk SSSR, No. 104 (1992), pp. 3-15.
7. S. V. Stebnovskii and N. N. Chernobaev, "Energy threshold for impulsive destruction of a liquid volume," Zh. Prikl. Mekh. Tekh. Fiz., No. 1, 57-61 (1986).
8. N. N. Chernobaev, "Numerical modeling of the initial stage of cavitation failure of a liquid under shock wave loading," in: Dynamics of Continuous Media, Collected Studies [in Russian], Sib. Otdel. Akad. Nauk SSSR, No. 83 (1987), pp. 128-137.